A Vortex Relocation Method for Improving Initial Conditions and Subsequent Predictions of Tornadoes

QIN XU,[a] KANG NAI,[a,b] LI WEI,[b] NATHAN SNOOK,[c] YUNHENG WANG,[a,b] AND MING XUE[c]

[a] *NOAA/OAR/National Severe Storms Laboratory, Norman, Oklahoma*
[b] *Cooperative Institute for Severe and High-Impact Weather Research and Operations, University of Oklahoma, Norman, Oklahoma*
[c] *Center for Analysis and Prediction of Storms, University of Oklahoma, Norman, Oklahoma*

ABSTRACT: A time–space shift method is developed for relocating model-predicted tornado vortices to radar-observed locations to improve the model initial conditions and subsequent predictions of tornadoes. The method consists of the following three steps. (i) Use the vortex center location estimated from radar observations to sample the best ensemble member from tornado-resolving ensemble predictions. Here, the best member is defined in terms of the predicted vortex center track that has a closest point, say at the time of $t = t^*$, to the estimated vortex center at the initial time t_0 (when the tornado vortex signature is first detected in radar observations). (ii) Create a time-shifted field from the best ensemble member in which the field within a circular area of about 10-km radius around the vortex center is taken from $t = t^*$, while the field outside this circular area is transformed smoothly via temporal interpolation to the best ensemble member at t_0. (iii) Create a time–space-shifted field in which the above time-shifted circular area is further shifted horizontally to co-center with the estimated vortex center at t_0, while the field outside this circular area is transformed smoothly via spatial interpolation to the non-shifted field at t_0 from the best ensemble member. The method is applied to the 20 May 2013 Oklahoma Newcastle–Moore tornado case, and is shown to be very effective in improving the tornado track and intensity predictions.

SIGNIFICANCE STATEMENT: The time–space shift method developed in this paper can smoothly relocate tornado vortices in model-predicted fields to match radar-observed locations. The method is found to be very effective in improving not only model initial condition but also the subsequent tornado track and intensity predictions. The method is also not sensitive to small errors in radar-estimated vortex center location at the initial time. The method should be useful for future real-time or even operational applications although further tests and improvements are needed (and are planned).

KEYWORDS: Radars/Radar observations; Interpolation schemes; Forecasting techniques; Numerical weather prediction/forecasting; Short-range prediction

1. Introduction

It has been well demonstrated and successfully implemented in operational models that relocating a tropical cyclone (TC) or replacing it with a bogus vortex can significantly improve the model initial condition and subsequent prediction of the TC (Kurihara et al. 1993, 1995; Liu et al. 2000, 2020; Hsiao et al. 2010; Liou and Sashegyi 2012; Hendricks et al. 2011; Schwartz et al. 2013). Motivated by the success of vortex relocation and initialization developed for TCs, a time–space shift method is developed in this paper for relocating tornado vortices in model-predicted background fields to radar-observed locations to improve the initial conditions and subsequent predictions of tornado vortices.

For a model-predicted tornado vortex, the vortex location error is often much larger than the vortex core radius, which can cause large non-Gaussian and nonunimodal errors in the predicted background fields in and around the vortex area that are difficult to deal with in data assimilation. It is thus more important and necessary for a tornado vortex than for a tropical cyclone to reduce the vortex center location error (as a bias error) as much as possible; one method for achieving this is via vortex relocation. In this case, the vortex center location must be estimated as a function of height z above the ground at the initial time t_0 of model integration. The estimated center location, denoted by $\mathbf{x}_c(z, t_0)$ with $\mathbf{x}_c \equiv (x_c, y_c)$, must be sufficiently accurate with an error smaller than the vortex core radius (i.e., the radius of the maximum tangential velocity). Since t_0 is set to (or nearly to) the time of tornado being first detected from radar observations and $\mathbf{x}_c(z, t_0)$ is estimated from observations on different tilts of radar scan (and thus on different vertical levels) at and after t_0, there is a delay from t_0 for performing vortex relocation due to observation latency.

For the 20 May 2013 Oklahoma Newcastle–Moore tornado considered in this paper, the three-step method of Xu et al. (2017) was used in Xu et al. (2022) to estimate $\mathbf{x}_c$ as a function of (z, t) up to $z = 5$ km over the entire time period that the tornado vortex was detected from the operational Oklahoma City, Oklahoma, radar (KTLX) and the NSSL phased-array radar (PAR). The estimated $\mathbf{x}_c(z, t)$ is sufficiently accurate, as assessed in Xu et al. (2022). However, since this estimate requires the observation data during the entire period of tornado vortex, it can only be applied for hindcast. In the current study, we modified the three-step method and used the

modified method to estimate $\mathbf{x}_c(z, t_0)$ from the earliest sweeps of radar scan that first detected the tornado vortex at different heights, so the observation latency can be minimized to an acceptable level (≤ 6 min). This estimated $\mathbf{x}_c(z, t_0)$ was applied to a forecast experiment and evaluated against a hindcast experiment using $\mathbf{x}_c(z, t_0)$ from Xu et al. (2022) in this study.

In each aforementioned experiment, the estimated $\mathbf{x}_c(z, t_0)$ was used to sample the best ensemble member from tornado-resolving ensemble predictions of the 20 May 2013 Oklahoma Newcastle–Moore tornado (Snook et al. 2019). We will show that the time–space shift method can be applied effectively to this best member to improve its initial conditions and subsequent prediction of the tornado in not only the hindcast experiment but also the forecast experiment.

The three-step method (Xu et al. 2017) is reviewed briefly first in the next section followed by detailed descriptions of the required modifications in the remaining part of the section. The time–space shift method is described in section 3, and the method is applied to the 20 May 2013 Oklahoma Newcastle–Moore tornado in section 4. The impact of the time–space shift on tornado track and intensity predictions is presented and examined in section 5. Conclusions follow in section 6.

2. Three-step method and modified method for estimating vortex center location

In the three-step method of Xu et al. (2017), the first step estimates $\mathbf{x}_c$ on each sweep of radar scan (as a by-product of the mesocyclone-targeted de-aliasing of Xu and Nai 2017) to generate a discrete dataset of $\mathbf{x}_{ci} = \mathbf{x}_c(z_i, t_i)$ at M irregularly distributed points in (z, t), where (z_i, t_i) denotes the ith irregularly distributed point and M is the total number of irregularly distributed points. The second step estimates $\mathbf{x}_c$, as a continuous function of (z, t), by fitting an expansion of B-spline basis functions to $\mathbf{x}_{ci}$ generated at (z_i, t_i) in the first step. The third step refines the second-step estimated $\mathbf{x}_c(z, t)$ by applying a continuous version of statistical interpolation to the residuals of the second-step fitting and adding the obtained incremental field to the second-step estimated $\mathbf{x}_c(z, t)$.

For the 20 May 2013 Oklahoma Newcastle–Moore tornado considered in this paper, $\mathbf{x}_c(z, t)$ has been estimated, up to $z = 4$ km (or 5 km) as shown in Fig. 1 of Xu et al. (2017) (or Fig. 2 of Xu et al. 2022), by applying the three-step method to dealiased radial velocities from the KTLX radar and PAR over the entire time window from 1951:42 to 2033:44 UTC during which the tornado vortex was detected. Since the error of the estimated $\mathbf{x}_c(z, t)$ is no more than 0.3 km, which is merely half of the vortex core radius (as assessed in section 6 of Xu et al. 2022), the estimated $\mathbf{x}_c(z, t_0)$ can represent true $\mathbf{x}_c(z, t_0)$ at the initial time t_0 (1950 UTC) and will be used as a benchmark $\mathbf{x}_c(z, t_0)$ for vortex relocation at t_0. This benchmark $\mathbf{x}_c(z, t_0)$, however, is estimated by using radar observations up to 2033:44 UTC (nearly 44 min delayed from t_0 at 1950 UTC), so its produced vortex relocation at t_0 and subsequent 40-min prediction constitute merely a hindcast experiment, named HC-Exp, in this paper.

For a forecast experiment, named FC-Exp, $\mathbf{x}_c(z, t_0)$ must be estimated on the earliest sweeps of radar scan that first detected the tornado vortex at different heights, so the observation latency can be minimized to an acceptable level. To achieve this, we need to apply the first step of the three-step method only to the earliest single volume scan (that is., the KTLX volume scan from 1951:42 to 1954:25 UTC) that first detected the tornado vortex at different heights (up to 5 km). This generates a discrete dataset of $\mathbf{x}_{ci}$ along the discrete trajectory of (z_i, t_i) but the total number of discrete points is reduced to $M = 10$ (from 319), so this discrete dataset is too sparse in (z, t) for properly estimating $\mathbf{x}_c(z, t)$ in the subsequent two steps of the three-step method.

To overcome the difficulty caused by the sparseness of $\mathbf{x}_{ci}$ in (z, t), we need to consider t in $\mathbf{x}_c(z, t)$ implicitly as a smooth function of z, denoted by $t = \tau(z)$, which can be a quadratic function of z but should fit closely the discrete trajectory of (z_i, t_i). We can then modify the three-step method by reducing the second-step fitting and third-step statistical interpolation in (z, t) to their respective one-dimensional versions in z, so these two steps can be used to estimate $\mathbf{x}_c[z, \tau(z)]$ as a function of z. To finally estimate $\mathbf{x}_c(z, t_0)$, we also need to estimate the vortex moving velocity by $\mathbf{u}_c = (\mathbf{x}_{cM+1} - \mathbf{x}_{c1})/(t_{M+1} - t_1)$, where $\mathbf{x}_{c1}$ and $\mathbf{x}_{cM+1}$ are the vortex center locations estimated at the lowest tilt (0.5° elevation) in the earliest and subsequent volume scans (from KTLX at $t_1 = 1951:42$ UTC and $t_{M+1} = 1955:59$ UTC, respectively). This gives $\mathbf{u}_c = (3.86, 3.67)$ m s^{-1}, so $\mathbf{x}_c(z, t_0)$ can be estimated by $\mathbf{x}_c[z, \tau(z)] - [\tau(z) - t_0]\mathbf{u}_c$. In this case, radar observations are used up to 1955:59 UTC, which is less than 6 min delayed from t_0 at 1950 UTC. This delay (<6 min due to observation latency) is acceptable for a 40-min forecast, so the estimated $\mathbf{x}_c(z, t_0)$ can be used in FC-Exp.

The error of estimated $\mathbf{x}_c(z, t_0)$ in FC-Exp can be assessed by its difference from the benchmark $\mathbf{x}_c(z, t_0)$ estimated in HC-Exp. By comparing the tornado track and intensity predictions in FC-Exp versus those in HC-Exp, we can evaluate the sensitivity of the time–space shift method to errors in the estimation $\mathbf{x}_c(z, t_0)$.

3. Description of the time–space shift method

The time–space shift method performs three steps to (i) sample the best ensemble member, (ii) temporally shift the best member such that its tornado track can be closest to radar-estimated $\mathbf{x}_c(z, t_0)$ at $z = 10$ m, and (iii) further shift the best member horizontally to move its tornado vortex center to radar-estimated location on each vertical level. The detailed procedures of these three steps are described below:

(i) Use the radar-estimated vortex center location at $z = 10$ m (i.e., the first model level above the surface) to sample the best ensemble member from tornado-resolving ensemble predictions initialized (say, 20 min earlier) before t_0. Here, the best member is defined in terms of its produced vortex center track that has a closest point, occurring at $t = t^*$ (which can be at any time during the forecast track), to the estimated vortex center at the initial time t_0. The vortex
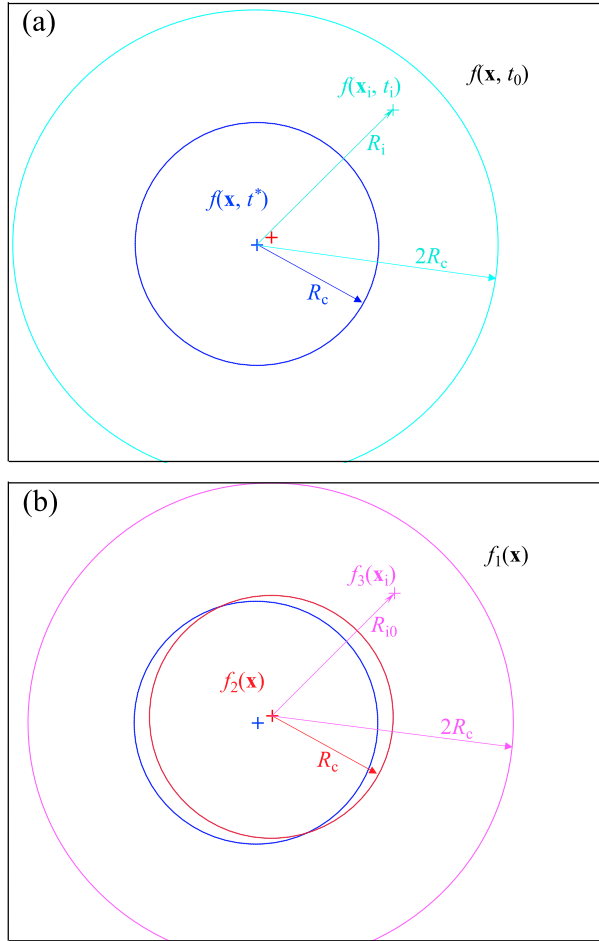
FIG. 2. Vortex center $\mathbf{x}_c$ from the best ensemble member run valid at $t = t^*$ marked sequentially by the blue line connecting the blue stars as a function of z_k with k increasing from 1 to 22, where z_k is the height of the model kth vertical level above the ground. The red line connecting the red plus signs (or green line connecting the green $\times$ signs) marks the radar-estimated $\mathbf{x}_c(z_k,)$ at t_0 in HC-Exp (or FC-Exp), also sequentially, as a function of z_k with k increasing from 1 to 22.

taking the best-member produced field valid at t^* (or t_0) within the radius of $R_c \approx 10$ km (or outside the $2R_c$ radius) from its produced vortex center at t^*, as illustrated in Fig. 1a. The field between R_c and $2R_c$ radii is given by the best-member produced field valid at a radial-distance-dependent intermediate time (between t^* and t_0) defined by

$$ t_i \equiv t^* + (t_0 - t^*)(R_i - R_c)/R_c, \qquad (1) $$

where R_i is the radial distance of the concerned grid point between the R_c and $2R_c$ radii from the best-member produced vortex center valid at t^* (see Fig. 1a). The linear temporal interpolation in (1) ensures that the field valid at t^* changes continuously to the field valid at t_0 as R_i increases from R_c to $2R_c$. The time-shifted field created in this step is denoted by $f_1(\mathbf{x})$.

(iii) Further shift $f_1(\mathbf{x})$ horizontally with the vortex center of $f_1(\mathbf{x})$ shifted to the estimated vortex center at t_0 on each vertical level. Denote this further horizontally shifted field by $f_2(\mathbf{x})$. Create a time–space-shifted field by taking $f_2(\mathbf{x})$ [or $f_1(\mathbf{x})$] within the radius of $R_c \approx 10$ km (or outside $2R_c$ radius) from the estimated vortex center at t_0, while the field between R_c and $2R_c$ radii is given by

$$ f_3(\mathbf{x}_i) = (R_{i0} - R_c)f_1(\mathbf{x}_i)/R_c + (2R_c - R_{i0})f_2(\mathbf{x}_i)/R_c, \quad (2) $$

where R_{i0} is the radial distance of the concerned grid point $\mathbf{x}_i$ (between R_c and $2R_c$ radii) from the estimated vortex center valid at t_0, as illustrated in Fig. 1b. The linear spatial interpolation in (2) ensures that $f_3(\mathbf{x})$ changes continuously from $f_2(\mathbf{x})$ to $f_1(\mathbf{x})$ as R_{i0} increases from R_c to $2R_c$.

FIG. 1. Schematics of (a) time-shifted field and (b) further horizontally shifted field produced in steps ii and iii, respectively. The blue (or red) plus sign marks the best ensemble member predicted $\mathbf{x}_c$ at $t = t^*$ (or radar-estimated $\mathbf{x}_c$ at $t = t_0$), the blue (or cyan) circle shows the area within R_c (or $2R_c$) radius from the blue plus sign, and the red (or purple) circle shows the area within R_c (or $2R_c$) radius from the red plus sign. In (a), the field within the blue circle, denoted by blue $f(\mathbf{x}, t^*)$, is time shifted from t^*; the field between the blue and cyan circles, denoted by cyan $f(\mathbf{x}_i, t_i)$ at point $\mathbf{x}_i$ (marked by the cyan plus sign with its distance from the blue plus sign denoted by cyan R_i), is time shifted from t_i defined in (1); and the field outside the cyan circle, denoted by black $f(\mathbf{x}, t_0)$, is not time shifted. In (b), the field within the red circle, denoted by red $f_2(\mathbf{x})$, is horizontally shifted from that within the blue circle in (a); the field outside the purple circle, denoted by black $f_1(\mathbf{x})$, is not shifted; and the field between the red and purple circles, denoted by purple $f_3(\mathbf{x}_i)$ at point $\mathbf{x}_i$ (marked by the purple plus sign with its distance from the red plus sign denoted by purple R_{i0}), is a linear combination of $f_1(\mathbf{x}_i)$ and $f_2(\mathbf{x}_i)$ as formulated in (2).

center track is produced at $z = 10$ m with the vortex center located every minute, while the vortex center is detected by and set to the grid point where the pressure perturbation reaches the minimum and the vorticity reaches the maximum or nearly so.

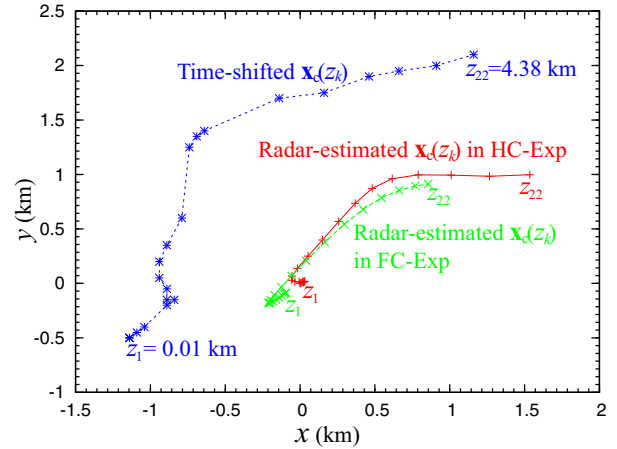(ii) Create a time-shifted field for each model variable at each vertical level from the best ensemble member by
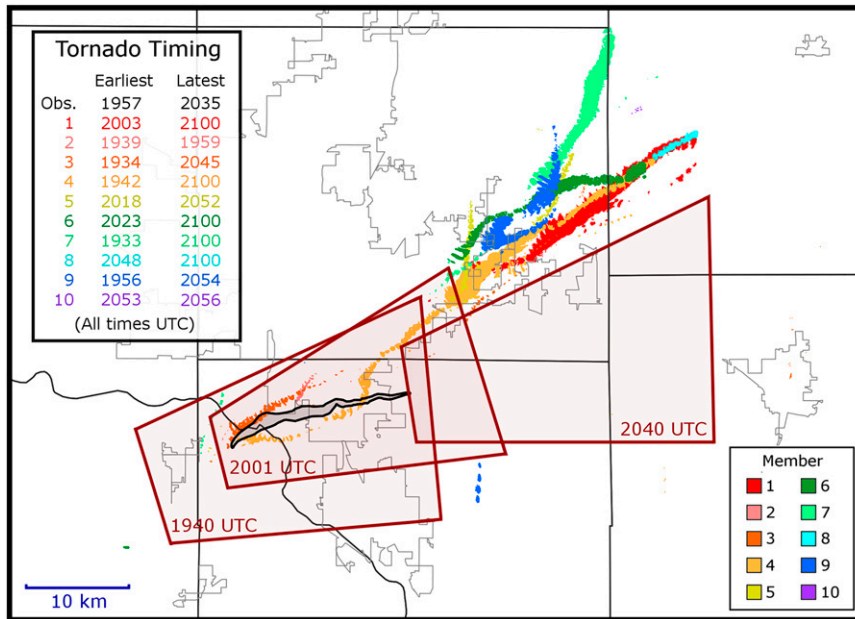
Fig. 3. Swaths of wind speed exceeding the EF0 threshold (29 m s^{-1}) at the first model level above the surface for each of the 10 members of the 50-m ensemble runs initialized at 1930 UTC, color coded by ensemble member. Urban areas are outlined in gray, county boundaries are denoted by thin black lines, and the observed extent of EF0 or greater damage from the Newcastle–Moore tornado is indicated by a thick black contour. Tornado warnings issued between 1930 and 2100 UTC by the NWS Norman WFO, labeled by time of issuance, are plotted (dark red boxes) for comparison. The earliest and latest times at which tornadoes were present for the observed tornado (Obs.) and for each member (1–10) are listed in the top-left inset as a general reference for timing. [Reprinted with permission from Snook et al. (2019).]

The above described three-step procedures can be simplified by skipping step (ii). In this case, $f_3(\mathbf{x})$ is still given by (2), but $f_1(\mathbf{x})$ is given directly by the best-member produced field valid at t_0 while $f_2(\mathbf{x})$ is given by the best-member produced field valid at t^* after the entire field is horizontally shifted with its vortex center moved to radar-estimated location at t_0 on each vertical level. This simplification can reduce the computational cost but cause slightly more dynamic/thermodynamic inconsistencies between its produced fields of different model variables over the area between R_c and $2R_c$ radii from the radar-estimated vortex center. This simplified approach will be considered/examined in our continued studies beyond this paper.

4. Application to 20 May 2013 Moore tornado

For the 20 May 2013 Oklahoma Newcastle–Moore EF5 tornado, as shown in Fig. 2, the radar-estimated $\mathbf{x}_c(z, t_0)$ in FC-Exp is very close to the benchmark $\mathbf{x}_c(z, t_0)$ estimated in HC-Exp, especially at $z = 10$ m. Using the radar-estimated $\mathbf{x}_c(z, t_0)$ at $z = 10$ m in either HC-Exp or FC-Exp, the ensemble member 3 is sampled consistently as the best one from the tornado-resolving (50 m) ensemble predictions initialized at 1930 UTC, as shown in Fig. 3 (duplicated from Fig. 3 of Snook et al. 2019). The reflectivity field from the best ensemble member run valid at $t = t_0$ (or $t = t^* = 1936{:}20$ UTC) is shown at $z = 10$ m by the color shades in Fig. 4a (or Fig. 4b), where

the blue plus sign marks the associated vortex center at $z = 10$ m for $t = t_0$ (or $t = t^*$) from the best ensemble member run, the red plus sign marks the radar-estimated benchmark $\mathbf{x}_c(z, t_0)$ at $z = 10$ m in HC-Exp, and the black contours show the areas of radar-observed reflectivity above 30 dBZ at $z = 10$ m and $t = t_0$.

As shown in Fig. 4a, the vortex center from the best ensemble member run valid at t_0 is about 10 km northeast of the radar-estimated benchmark vortex center and the associated hook-echo area of reflectivity is also about 10 km northeast of the radar observed. However, as shown in Fig. 4b, the vortex center from the best ensemble member run valid at $t = t^*$ (13 min 40 s earlier than t_0) is very close to the radar-estimated benchmark vortex center at t_0 and the associated hook-echo area of reflectivity also matches closely the radar observed at t_0. In fact, on the vortex center track produced by the best ensemble member run, the vortex center valid at t^* is closest to the radar-estimated benchmark vortex center at t_0, which is consistent with the definition of best member given in step i of section 3. The field produced for each model variable by the best ensemble member run valid at t^* in the circular area within the thin blue circle (of $R_c = 9$-km radius) in Fig. 4b is thus used to replace the field of the same model variable valid at t_0 over the same circular area (see the reflectivity field within the thin blue circle in Fig. 4c). As described in step ii of section 3, the field between R_c and $2R_c$ radii is transformed
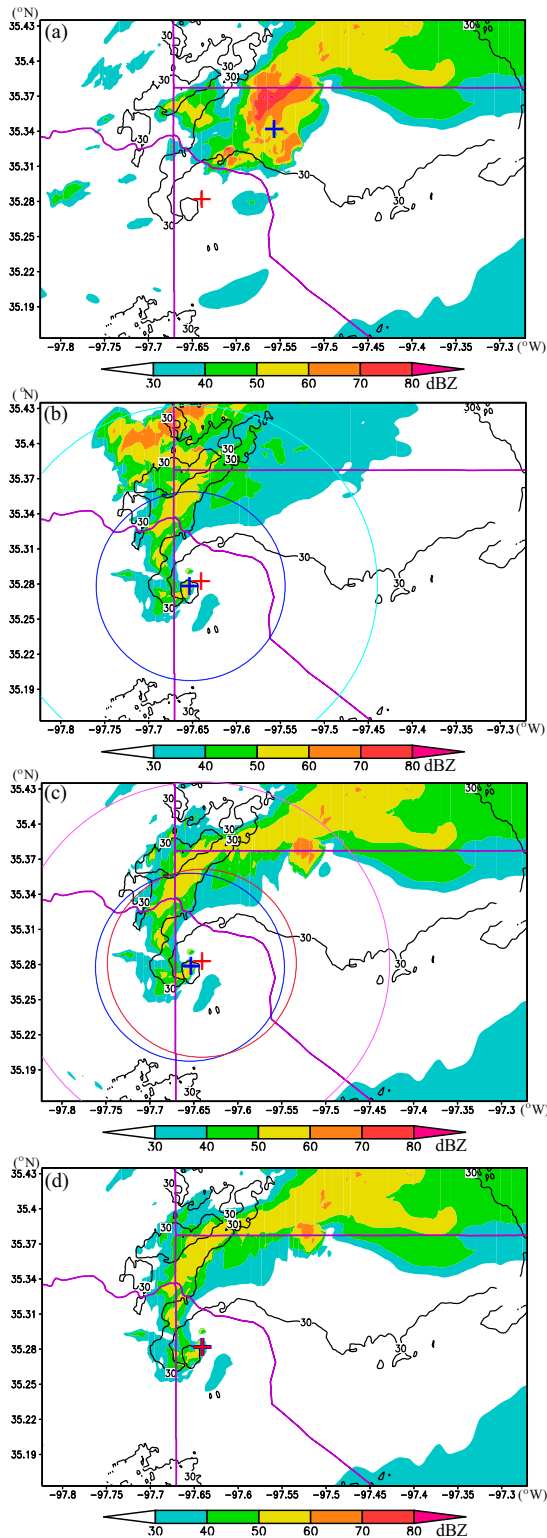
FIG. 4. (a) Reflectivity field from the best ensemble member run shown by the color shades and associated vortex center marked by the blue plus sign at $z = 10$ m valid at $t = t_0 = 1950$ UTC. (b) As in (a), but valid at $t = t^* = 1936:20$ UTC. (c) As in (a), but for the time-shifted reflectivity field produced in step ii in HC-Exp.

continuously from the field of t^* inside R_c radius to the field of t_0 outside $2R_c$ radius by using the temporal interpolation in (1). This time shift is performed in step ii for each model variable on each vertical level up to the highest possible vertical level (i.e., $k = 22$ at $z = 4.38$ km for the case presented here) where the radar-estimated $\mathbf{x}_c(z, t_0)$ and the best-member-produced $\mathbf{x}_c$ at t^* are both available. For higher vertical levels from $k = 23$ to 63 (at the model top), the time shift is performed in the same way as that for the vertical level of $k = 22$. The time-shifted reflectivity field produced in step ii is shown at $z = 10$ m in Fig. 4c for HC-Expt, which is visually indistinguishable from that (not shown) for FC-Expt.

The time–space-shifted reflectivity field produced in step iii in HC-Expt is shown at $z = 10$ m in Fig. 4d. In this step, the time-shifted vortex center marked by the blue plus sign in Fig. 4c is further shifted horizontally to collocate with the radar-estimated vortex center at t_0, while the circular area within the thin blue circle in Fig. 4c is also shifted horizontally with the vortex center. As shown in Fig. 4d, the hook-echo area of the time–space-shifted reflectivity field matches the radar observed more closely than that in Fig. 4c for the time-shifted reflectivity field within the thin blue circle. As described in step iii of section 3, the field outside the horizontally shifted circular area of R_c radius (see the thin red circle in Fig. 4c) is transformed continuously to the field outside the circle of $2R_c$ radius (see the thin purple circle in Fig. 4c) by using the spatial interpolation in (2). This horizontal space shift is performed in step iii for each model variable on each vertical level, again, up to the highest vertical level of $k = 22$ (at $z = 4.38$ km) where the radar-estimated $\mathbf{x}_c$ at t_0 and the best-member-produced $\mathbf{x}_c$ at t^* are both available. For higher vertical levels (from $k = 23$ to 63), the horizontal shift is performed in the same way as that for the vertical level of $k = 22$. Figure 2 shows how the predicted $\mathbf{x}_c$ valid at t^* (marked by blue star signs) is shifted horizontally to the radar-estimated $\mathbf{x}_c$ at t_0 (marked by green $\times$ signs) in FC-Exp or to the radar-estimated benchmark $\mathbf{x}_c$ at t_0 (marked by red plus signs) in HC-Exp on each of the 22 vertical levels.

The surface winds (at $z = 10$ m) from the best ensemble member run valid at $t = t_0 = 1950$ UTC are shown by black arrows in Fig. 5a. As shown, the surface winds are rotating cyclonically and converging toward the vortex center (marked by the blue plus sign), but the vortex center valid at $t = t_0$ is about 10 km northeast of the radar-estimated vortex center at

←
(d) As in (c), but for the time–space-shifted reflectivity field produced in step iii. In each panel, the black contours show the areas of radar-observed reflectivity above 30 dBZ at $z = 10$ m and $t = t_0$, the red plus sign marks the radar-estimated benchmark $\mathbf{x}_c(z, t_0)$ at $z = 10$ m in HC-Exp, and the thin purple lines show county boundaries. In (b), the thin blue (or cyan) circle shows the circular area within the radius of $R_c = 9$ km (or $2R_c$) around the vortex center (marked by the blue plus sign) from the best ensemble member run valid at $t = t^*$. In (c), the thin red (or purple) circle shows the circular area within the radius of R_c (or $2R_c$) around the radar-estimated benchmark vortex center (marked by the red plus sign) in HC-Exp and the thin blue circle duplicates that in (b).
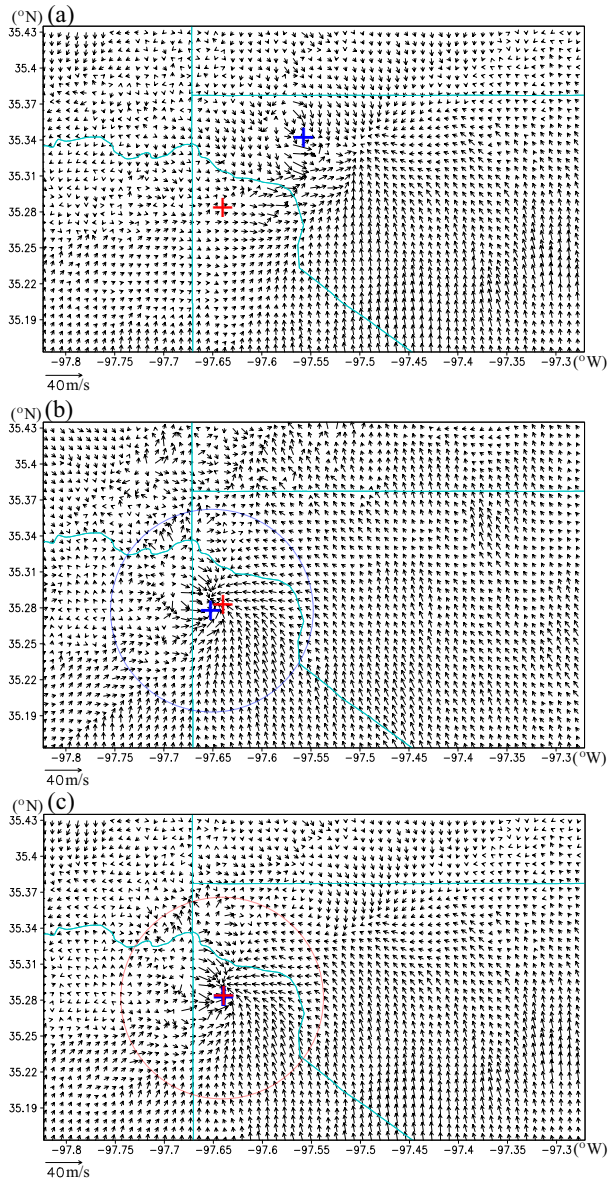
FIG. 5. (a) Surface winds (at $z = 10$ m) from the best ensemble member run plotted by black arrows with the associated vortex center marked by the blue plus sign valid at $t = t_0 = 1950$ UTC. (b) As in (a), but valid at $t = t^* = 1936:20$ UTC. (c) As in (a), but for the time–space-shifted velocity field produced in step iii in HC-Exp. In each panel, the red plus sign marks the radar-estimated benchmark vortex center at $z = 10$ m and $t = t_0 = 1950$ UTC in HC-Exp, and the thin cyan lines show county boundaries.

$t = t_0$ (marked by the red plus sign), which is the same as seen previously from Fig. 4a. On the other hand, as shown in Fig. 5b, the surface winds from the best ensemble member run valid at $t = t^* = 1936:20$ UTC are strongly convergent and rotating cyclonically around the vortex center (marked by the blue plus sign), and the vortex center valid at this time ($t = t^*$) is very close to the radar-estimated vortex center at t_0 (marked by the red plus sign), as seen previously from Fig. 4b.

Figure 5c shows the time–space-shifted surface winds produced in step iii in HC-Exp. As shown, the surface winds preserve the strong convergence and highly cyclonic rotation around the time–space-shifted vortex center that is now collocated with radar-estimated vortex center at t_0. The surface winds in Fig. 5c preserve not only the first rear-flank gust front (that is curved and extended southwestward) but also the second rear-flank gust front (that is curved and extended westward behind the first rear-flank gust front), as well as the extended zone of strong wind shift and convergence north of the vortex core (see Fig. 5c versus Fig. 5b). The time–space-shift also preserves the temperature and humidity variations across and along these frontal zones (not shown) in the vicinity of the vortex core.

The tornado vortex was first detected and visualized as a dipole of positive and negative radial velocities around the vortex center in the dealiased radial velocity image from the KTLX radar scan on 0.5° sweep at 1951:42 UTC (not shown). By projecting the predicted velocities from the best ensemble member valid at $t_0 = 1950$ UTC (or $t^* = 1936:20$ UTC) onto the KTLX radar beam directions on 0.5° sweep, the predicted vortex can be visualized by a dipole in the projected radial-velocity field around the vortex center (not shown). Similarly, the time–space-shifted vortex can be also visualized by a dipole around the time–space-shifted vortex center in its projected radial velocity field (not shown). By comparing the radar-observed dipole with those in the above three projected radial velocity fields, we find that (i) the best-member-predicted vortex valid at t_0 is slightly weaker and larger than the radar observed but the predicted vortex center is about 10 km northeast of the radar observed (as seen previously from Figs. 4a and 5a); (ii) the best-member predicted vortex valid at t^* is much less rotational but more convergent (at $z = 10$ m) than the radar observed while the predicted vortex center is very close to the radar observed (as seen previously from Figs. 4b and 5b); (iii) the time–space-shifted vortex preserves the vortex structure from the best-member predicted vortex valid at t^* while the vortex center is shifted to the radar-observed location; and (iv) the time–space-shifted vortex in FC-Exp is visually indistinguishable from that in HC-Exp.

5. Improved tornado track and intensity predictions

The time–space shift is performed for each model prognostic variable on the same tornado-resolving (50 m) grid as that used for the ensemble predictions initialized at 1930 UTC in Snook et al. (2019). To avoid complications caused by parallel computation, the time–space-shifted fields (for all the model prognostic variables) are coarsened from 50 to 100 m in the horizontal resolution and then used to reinitialize the model prediction at $t = t_0 = 1950$. Figure 6 shows that the predicted tornado track in HC-Exp (plotted by green filled circles) matches the observed track (plotted by black filled circles) much more closely than the predicted track from the best ensemble member without vortex relocation (plotted by blue × symbols). Figure 6 also shows that the predicted tornado track in FC-Exp (plotted by red open circles) is very close to the predicted track in HF-Exp, so the tornado track prediction
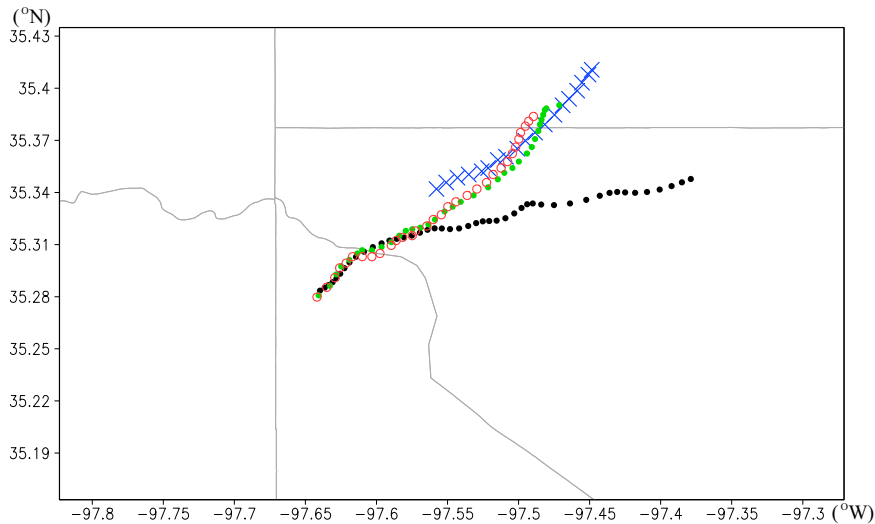
FIG. 6. Observed tornado track plotted by black filled circles (every minute from the initial time t_0 at 1950 UTC to 2035 UTC), predicted track from the best ensemble member without vortex relocation plotted by blue × signs (every minute from t_0 to 2008 UTC), predicted track in HC-Exp plotted by green filled circles (every minute from t_0 to 2024 UTC), and predicted track in FC-Exp plotted by red open circles (every minute from t_0 to 2021 UTC). The thin black lines show county boundaries.

produced with vortex relocation by using the time–space shift method is not sensitive to small errors in radar-estimated $\mathbf{x}_c(z, t_0)$ (see Fig. 2).

Figures 7a–d show the predicted surface winds in HC-Exp valid at the time of 5, 10, 15 and 20 min, respectively, after the vortex relocation. As shown in Fig. 7a versus Fig. 5c, during the first 5-min period into the forecast time, the predicted vortex center (marked by the blue plus sign) moves northeastward slightly faster than the vortex center estimated from radar observations (marked by the red plus sign). As the predicted vortex moves northeastward, it also becomes more intense at this time (1955 UTC) than that (see Fig. 5c) at the initial time of $t = t_0$ (1950 UTC), and so do the first and second rear-flank gust fronts as well as the northeastward extended zone of wind shift and convergence. In this case, the second rear-flank gust front is intensified but still not as intense as the first rear-flank gust front. During the second 5-min period into the forecast time, as shown in Fig. 7b versus Fig. 7a, the predicted vortex center moves mainly eastward and again slightly faster than the vortex center estimated from radar observations. Along with the predicted vortex movement, the first and second rear-flank gust fronts also move mainly eastward, and the second rear-flank gust front becomes more intense than the first gust front. During the third 5-min period into the forecast time, as shown in Fig. 7c versus Fig. 7b, the predicted vortex center moves farther northeastward and remains ahead of the vortex center estimated from radar observations. Along with the predicted vortex movement, the first and second gust fronts also move northeastward but become relatively weak while a third rear-flank gust front is generated behind (to the west of) the second gust front along the southern edge of the vortex core and

becomes stronger than the second gust front. During the fourth 5 min into the forecast time, as shown in Fig. 7d versus Fig. 7c, the predicted vortex center moves farther northeastward and again slightly faster than the vortex center estimated from radar observations. Along with the predicted vortex movement, the three gust fronts also move farther northeastward but all become weak, while the surface winds in the vortex core become strongly divergent.

The predicted surface wind fields in FC-Exp (not shown) valid at the time of 5, 10, 15, and 20 min, respectively, are almost the same as those shown in Figs. 7a–d, respectively, for HC-Exp. Thus, in line with the closeness of predicted tornado track in FC-Exp to that in HC-Exp shown in Fig. 6, the closeness of predicted wind field in FC-Exp to that in HC-Exp indicates that the wind prediction produced by using the time–space shift method is also not sensitive to small errors in radar-estimated $\mathbf{x}_c(z, t_0)$.

Figure 8a (or Fig. 8b) shows that the predicted maximum vorticity (or wind speed) at $z = 10$ m with the vortex relocation in either HC-Exp (plotted by the green curve) or FC-Exp (plotted by the red curve) is higher and lasts longer time than that predicted (plotted by the blue curve) without vortex relocation. Note that the time–space-shifted vortex preserves the best-member predicted vortex structure valid at $t = t^* = 1936{:}20$ UTC while the latter is much less rotational than the radar observed, so the predicted vortex intensity with the vortex relocation is still substantially weaker than the observed intensity of EF5 tornado. Here, the closeness of predicted tornado intensity in FC-Exp to that in HC-Exp further indicates that not only the tornado track prediction but also the intensity prediction produced by using the time–space shift method are not sensitive to small errors in radar-estimated $\mathbf{x}_c(z, t_0)$.
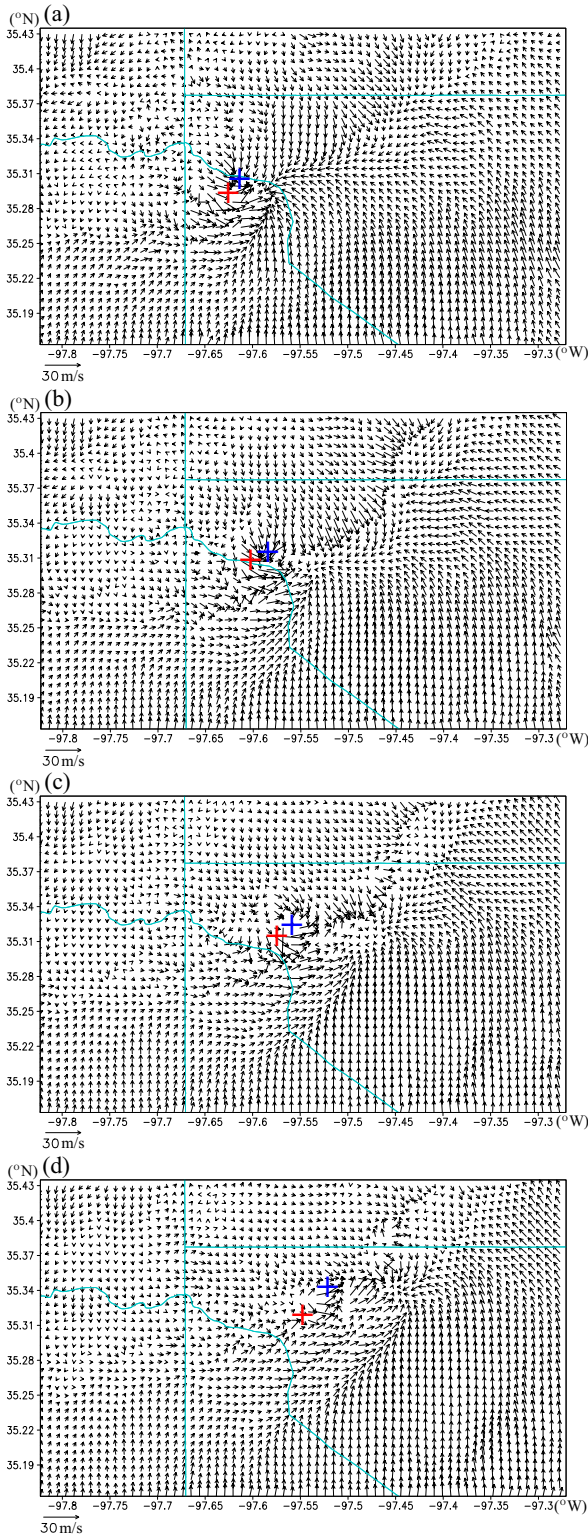
FIG. 7. (a) Predicted surface winds (at $z = 10$ m) after vortex relocation plotted by black arrows with the predicted vortex center marked by the blue plus sign valid at $t = t_0 + 5$ min (1955 UTC). (b) As in (a), but valid at $t = t_0 + 10$ min (2000 UTC). (c) As in (a), but valid at $t = t_0 + 15$ min (2005 UTC). (d) As in (a), but valid at
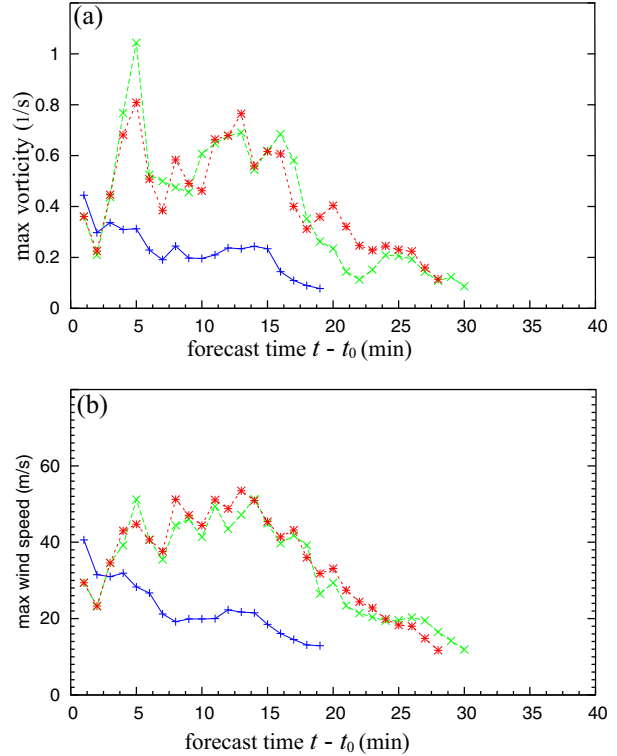

FIG. 8. (a) Time series of maximum vorticity (at $z = 10$ m) of tornado vortex predicted without vortex relocation at t_0 plotted by blue curve and predicted with vortex relocation at t_0 in HC-Exp (or FC-Exp) plotted by the green (or red) curve. (b) As in (a), but for time series of predicted maximum surface wind speed.

6. Conclusions

A time–space shift method is developed in this paper for relocating a model-predicted tornado vortex to the radar-observed location. The utility and effectiveness of the method are demonstrated by its application to the best ensemble member sampled from tornado-resolving ensemble predictions of 20 May 2013 Newcastle–Moore EF5 tornado in Oklahoma (Snook et al. 2019). In particular, the time–space shift method is applied to relocate the best-ensemble-predicted vortex center with each model-variable field in and around the vortex core to match the vortex center estimated, at the initial time t_0, from radar observations delayed 44 min (or nearly 6 min) from t_0 in a hindcast experiment, named HC-Exp (or a forecast experiment, named FC-Exp). In either experiment, the method is found and shown to be very effective in improving not only the intimal condition after the vortex relocation but also the subsequent tornado track and intensity prediction, although the predicted vortex intensity is still

←

$t = t_0 + 20$ min (2010 UTC). In each panel, the red plus sign marks the radar-estimated vortex center at $z = 10$ m valid at the same time as the predicted vortex center (marked by the blue plus sign), and the thin cyan lines show county boundaries.

substantially weaker than the observed intensity of EF5 tornado due mainly to the insufficient intensity in relocated vortex at the initial time.

The method is also found to be not sensitive to small errors in radar-estimated tornado vortex location at t_0, as indicated by the closeness of the predicted tornado track and intensity in FC-Exp to those in HC-Exp. However, the effectiveness of the method is likely to depend on or to be limited by the smallness of error in radar-estimated tornado vortex location. The effectiveness of the method may also depend whether the best-member predicted tornado track has a point (not necessarily at or close to t_0) sufficient close to radar-estimated vortex location at t_0. These potential limitations are not investigated yet in this paper.

The above summarized results also indicate that the vortex intensity prediction should and can be further improved by improving the initial vortex intensity after the vortex relocation. Since 3D high-resolution vortex winds can be retrieved by using the vortex-flow variational method, called VF-Var (Xu 2021; Xu et al. 2022), from radar radial velocity observations of tornadic mesocyclones, the retrieved 3D high-resolution vortex winds can be used as pseudo-observations and assimilated into the wind field after the vortex relocation to improve the initial vortex intensity and subsequent vortex intensity prediction. Continued research is conducted in this direction, and the results will be presented in a follow-up paper.

Finally, although the observation latency can be reduced to an acceptable level (≤6 min for the 40-min prediction in FC-Exp) and the CPU time for vortex relocation (including radar velocity de-aliasing and estimating the vortex center location) can be sufficiently short (<1 min), the method still faces another serious challenge for future real-time/operational applications on how to reduce the CPU time (currently 3.5 h) for the vortex-relocated 40-min prediction run. To reduce this CPU time to an acceptable level (<5 min), we must properly coarsen the horizontal resolution (say, from current 100 to 500 m with the horizontal grid size reduced from 503×303 to 101×61) so the tornado vortex is still resolvable. In this case, the ensemble prediction run (initialized 20 min before t_0) can be also coarsened (say, to 1-km resolution) to resolve just the mesocyclone but not the tornado, so its CPU time can be shorter or much shorter than 20 min and thus will cause no delay for the vortex-relocated prediction run initialized at t_0. Continued research is required and will be conducted in this direction.

REFERENCES

Hendricks, E. A., M. S. Peng, T. Li, and X. Ge, 2011: Performance of a dynamic initialization scheme in the Coupled Ocean–Atmosphere Mesoscale Prediction System for Tropical Cyclones (COAMPS-TC). *Wea. Forecasting*, **26**, 650–663, https://doi.org/10.1175/WAF-D-10-05051.1.

Hsiao, L.-F., C.-S. Liou, T.-C. Yeh, Y.-R. Guo, D.-S. Chen, K.-N. Huang, C.-T. Terng, and J.-H. Chen, 2010: A vortex relocation scheme for tropical cyclone initialization in Advanced Research WRF. *Mon. Wea. Rev.*, **138**, 3298–3315, https://doi.org/10.1175/2010MWR3275.1.

Kurihara, Y., M. A. Bender, and R. J. Ross, 1993: An initialization scheme of hurricane models by vortex specification. *Mon. Wea. Rev.*, **121**, 2030–2045, https://doi.org/10.1175/1520-0493(1993)121<2030:AISOHM>2.0.CO;2.

——, ——, R. E. Tuleya, and R. J. Ross, 1995: Improvements in the GFDL hurricane prediction system. *Mon. Wea. Rev.*, **123**, 2791–2801, https://doi.org/10.1175/1520-0493(1995)123<2791:IITGHP>2.0.CO;2.

Liou, C.-S., and K. D. Sashegyi, 2012: On the initialization of tropical cyclones with a three dimensional variational analysis. *Nat. Hazards*, **63**, 1375–1391, https://doi.org/10.1007/s11069-011-9838-0.

Liu, Q., T. Marchok, H. Pan, M. Bender, and S. Lord, 2000: Improvements in hurricane initialization and forecasting at NCEP with global and regional (GFDL) models. NCEP Office Note 472, 7 pp.

——, and Coauthors, 2020: Vortex initialization in the NCEP operational hurricane models. *Atmosphere*, **11**, 968, https://doi.org/10.3390/atmos11090968.

Schwartz, C. S., Z. Liu, X.-Y. Huang, Y.-H. Kuo, and C.-T. Fong, 2013: Comparing limited-area 3DVAR and hybrid variational-ensemble data assimilation methods for typhoon track forecasts: Sensitivity to outer loops and vortex relocation. *Mon. Wea. Rev.*, **141**, 4350–4372, https://doi.org/10.1175/MWR-D-13-00028.1.

Snook, N., M. Xue, and Y. Jung, 2019: Tornado-resolving ensemble and probabilistic predictions of the 20 May 2013 Newcastle–Moore EF5 tornado. *Mon. Wea. Rev.*, **147**, 1215–1235, https://doi.org/10.1175/MWR-D-18-0236.1.

Xu, Q., 2021: A variational method for analyzing vortex flows in radar scanned tornadic mesocyclones. Part I: Formulations and theoretical considerations. *J. Atmos. Sci.*, **78**, 825–841, https://doi.org/10.1175/JAS-D-20-0158.1.

——, and K. Nai, 2017: Mesocyclone-targeted Doppler velocity dealiasing. *J. Atmos. Oceanic Technol.*, **34**, 841–853, https://doi.org/10.1175/JTECH-D-16-0170.1.

——, L. Wei, and K. Nai, 2017: A three-step method for estimating vortex center locations in four-dimensional space from radar observed tornadic mesocyclones. *J. Atmos. Oceanic Technol.*, **34**, 2275–2281, https://doi.org/10.1175/JTECH-D-17-0123.1.

——, ——, and ——, 2022: A variational method for analyzing vortex flows in radar observed mesocyclones. Part IV: Applications to the 20 May 2013 Oklahoma tornadic mesocyclone. *J. Atmos. Sci.*, **79**, 1531–1547, https://doi.org/10.1175/JAS-D-21-0247.1.